Holey graphene with enhanced near-infrared absorption: Experimental and DFT study

O. V. Sedelnikova 🆔, S. G. Stolyarova 🆔, A. L. Chuvilin 🆔, A. V. Okotrub 🆔, and L. G. Bulusheva 🆔

View Online   Export Citation   CrossMark

ARTICLES YOU MAY BE INTERESTED IN

Holey graphene with enhanced near-infrared absorption: Experimental and DFT study

O. V. Sedelnikova,[1,2,a)] S. G. Stolyarova,[1] A. L. Chuvilin,[3,4] A. V. Okotrub,[1,2] and L. G. Bulusheva[1,2]

AFFILIATIONS

[1]Nikolaev Institute of Inorganic Chemistry, SB RAS, 3 Acad. Lavrentiev Ave., 630090 Novosibirsk, Russia
[2]Novosibirsk State University, 2 Pirogov Str., 630090 Novosibirsk, Russia
[3]CIC nanoGUNE, Tolosa Hiribidea 76, 20018 Donostia-San Sebastián, Spain
[4]IKERBASQUE, Basque Foundation for Science, Maria Diaz de Haro 3, 48013 Bilbao, Spain

[a)]Author to whom correspondence should be addressed: o.sedelnikova@gmail.com

ABSTRACT

In this report, we use optical absorption spectroscopy and density functional theory simulations to investigate the optical behavior of a graphitic material with nanoscale holes. The material, produced by heating of graphite oxide in concentrated sulfuric acid followed by annealing at $1000\,°C$, demonstrated enhanced near-infrared absorption as compared to the pristine graphitic material. The computational study of graphene models containing holes of different sizes and different edge terminations revealed the major interband transitions defining the peaks in the absorption spectra. Our results suggest that the enhancement of near-infrared absorption of the material is caused by electron excitations involving hole edge states. The optical spectrum is strongly dependent on the distance between the holes and almost independent of both hole sizes and the functionalization family.

Holey graphene (HG), also called "graphene antidote lattice" and "graphene mesh," is a structural derivative of graphene possessing specific physical and chemical properties.[1] HG is a two-dimensional material with abundant vacancy defects (or holes) distributed in the honeycomb lattice. HG can be produced using nanolithography and templates[1] or by electron irradiation of a graphene layer.[2] The main method for gram-scale production of HG is a heat treatment of graphite oxide (GO) in the presence of a reducing agent.[1] At low temperatures, GO interacts with acids or acetonitrile via the dehydration reaction, which mainly restores the graphitic sheets.[3,4] In turn, hot mineral acids act simultaneously as defunctionalizing and etching agents and the removal of lattice carbon atoms creates nanoscale holes.[4–9] Being very reactive, the hole edges are readily decorated by oxygen- and hydrogen-containing functional groups.

HG has fascinating electronic properties due to the quantum confinement effects. Theoretical calculations predict that perforation of the graphene lattice could open a finite bandgap[10–15] that leads to an increase in the on-off current ratio observed experimentally.[16–21] On the other hand, formation of the electronic subbands in HG near the Fermi level should enhance the infrared absorption that is beneficial for optoelectronic applications of graphene.

A few existing works discussing evolution of optical response of GO under reduction processes[22–25] analyze mostly the influence of the oxygen content on the absorbance and do not consider the contribution of holes themselves. One can associate this oversight with the abundance of oxygen-containing groups decorating the holes, which may conceal the contribution of the hole edges in the HG absorption.

In this work, we aim to fill this niche and investigate the effect of nanoscale holes including their functionalization on the optical properties of HG using optical absorption spectroscopy and density functional theory (DFT) calculations. The HG material was obtained from a natural graphite from Zavalievo deposit following the procedure[9] briefly described below. At first, natural graphite was oxidized using a modified version of the Hummer's method.[26] The thus-obtained GO ($\sim 0.5\,g$) was suspended in $100\,ml$ of concentrated sulfuric acid and the suspension was heated in a glass flask at $280\,°C$ for 1 h and then naturally cooled to room temperature. The obtained black powder was washed with distilled water to pH ~ 6 and dried under ambient conditions. As we have shown previously,[7] the as-prepared material is holey reduced GO (HRGO) due to the appearance of abundant oxygenated vacancy defects in the graphene lattice. Finally, annealing of the HRGO powder in an argon flow at $1000\,°C$ for 1 h produced the HG sample.[9] X-ray photoelectron spectroscopy (XPS) analysis has shown that the high-temperature annealing of the HRGO reduces the total oxygen content from 13.0 to 1.6 at. %.[9] The residual oxygen was associated with ether and ketonic groups, which have a high thermal

stability. Thermally exfoliated graphite (TEG), prepared from a graphite intercalation compound, and HRGO before annealing were taken as reference materials. The details of the synthesis and characterization of the TEG sample can be found in Ref. 27. Briefly, TEG was obtained by fast heating of the graphite intercalation compound with nitric and sulfuric acids at 800 °C.[28] The compound decomposes into graphene flakes with a lateral size of ∼1 μm.[27]

HG was studied by high-resolution transmission electron microscopy (HR TEM) on a Titan 60–300 electron microscope (FEI, Netherlands) equipped with an image side Cs spherical aberration corrector and monochromator. The images were obtained at an accelerating voltage of 80 kV, beam monochromated to about 0.1 eV energy spread, a Cs value of −25 μm, and positive defocus. Figure 1(a) presents a typical HR TEM image, which confirms the formation of nanoscale holes in the layers. The characteristic size of the holes is ca. 2 nm and the distance between them varies from 2 to about 4 nm. The smeared 6-fold pattern on the fast Fourier transform (FFT), obtained for the HR TEM image, evidences high local misorientation of the lattice yet preserving far order of the graphene, which is typical for reduced graphene oxide.[2]

Optical absorption spectra of TEG, HRGO, and HG were recorded on a Shimadzu UV 3101 PC spectrometer in a range of 190–1200 nm. Powder samples were dispersed in isopropanol by a treatment for 30 min in an ultrasonic bath (110 W). The dispersions obtained were sprayed onto quartz substrates heated to 100 °C. The thickness and uniformity of the prepared films were controlled visually.

The absorption spectra of the three samples are compared in Fig. 1(b). The peak located at 266 nm (4.66 eV) in the spectrum of TEG is attributed to $\pi \rightarrow \pi^*$ electron transitions for the sp^2-hybridized carbon layer.[27,29,30] Normally, when graphite is oxidized, this peak blueshifts to ca. 230 nm (5.40 eV) due to the preservation of small sp^2 domains. Reduction of GO restores large-areas of the conjugated π-electron system and this causes a redshift of the absorption peak back to its position in the bare graphite material.[24] The $\pi \rightarrow \pi^*$ peak values in the spectra of HRGO and HG are 276 and 282 nm (4.50 and 4.40 eV), respectively, which are slightly more (less) than the corresponding value for TEG. Earlier, a similar redshift of the π-band of onion-like carbon was attributed to the corrugation of the graphene layer[27,29,30] that could occur between the neighboring vacancy defects.

Weak features observed in the spectra of TEG and HRGO between 300 and 1200 nm (4.13–1.03 eV) can be assigned to residual
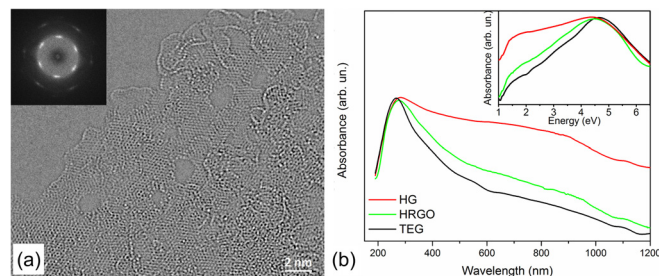
oxygen-containing functional groups. Previous calculations have shown that the attachment of oxygen-containing groups to basal graphene plane produces absorption bands, whose positions gradually shift from the IR to UV region with an increase in the oxidation level.[25] In particular, the graphene layer with the oxygen loading of 40 at. % and 44 at. % has absorption edges at about 1 and 4 eV, respectively. In the case of the HG material with a low content of oxygen, the low-energy features, whose intensities become comparable with the π-band intensity, should have another origin. A theoretical study of graphene with hexagonal holes has mentioned the appearance of additional low-energy absorption peaks;[15] however, they have not been analyzed in detail.

We constructed the models with hexagonal-shaped holes periodically distributed along armchair directions of the graphene plane. Translation vectors of the hexagonal supercell had a length of 1.28 nm. The separation of sheets was 2 nm. The holes were obtained by the removal of one hexagon (6 atoms) or coronene-like polycycle (24 atoms) from the supercell. The edges of the holes were naked in model 6-HG [Fig. 2(a-I)] and saturated with hydrogen atoms in models 6H-HG [Fig. 2(b-I)] and 24H-HG [Fig. 2(c-I)]. Taking into account the XPS data, one ether oxygen atom [model 6O^{ether}-HG in Fig. 2(d-I)] or two ketonic oxygen atoms [model 24O^{ketonic}-HG in Fig. 2(e-I)] were placed on the hole edge instead of two hydrogen atoms. To study the effect of the width of graphene neck on the absorption spectrum of HG, we increased distance between hydrogenated 24-atom vacancies (the hexagonal supercell had a length of 1.7 nm). The obtained model was denoted as 24H-HG* (see supplementary material for details).

The electronic ground-state structure of graphene and HG models was obtained using the plane-wave self-consistent field formalism in the local density approximation as implemented in the Quantum-ESPRESSO code.[31] The Kohn-Sham orbitals were expanded using plane waves with a kinetic energy cutoff of 30 Ry. The interaction between the valence electrons and the ionic core was described by a norm-conserving pseudopotential in the Perdew-Zunger parametrization.[32] For self-consistent and density of states (DOS) calculations, the unshifted k-point grid was $20 \times 20 \times 1$ and $40 \times 40 \times 1$, respectively. The atomic positions of all atoms were optimized within the Broyden-Fletcher-Goldfarb-Shanno method[33] until forces were below 10^{-3} a.u., while the cell size was constant. Earlier, we have demonstrated that band electronic structures[34,35] of graphene- and graphite-based materials calculated using the applied approach are in good agreement with theoretical and experimental data. The optimized HG models are almost flat. The displacement (d) of atoms located at the hole edges from the basal plane is less than 0.003 nm except the 24O^{ketonic}-HG model, where $d \approx 0.11$ nm [inset in Fig. 2(e-I)].

Figure 2 summarizes the calculated band structures (column II) and the projected DOS (PDOS, column III) for the models. It can be seen that the 6-HG model is metallic [inset in Fig. 2(a-II)], while the others are direct band-gap semiconductors in agreement with the previous results.[10–14] The decrease in the size of the hole or attachment of oxygen atoms to the hole edges reduces the bandgap. So, the controlled oxidation of holes can tune the bandgap of the HG material.

Analysis of PDOS of the HG models allows us to distinguish three groups of the bands. The first group includes flat bands (highlighted in purple, green, and red colors in Fig. 2-II). They are contributed by unpaired electrons of naked hole edges (p_{xy}^{hole} at the Fermi level of the 6-HG model), localized electrons of C=O bonds

FIG. 1. HR TEM image of HG and the FFT pattern of the image (a). Optical absorption spectra of HG, HRGO, and TEG (b). The inset shows the same graphs on the energy scale.
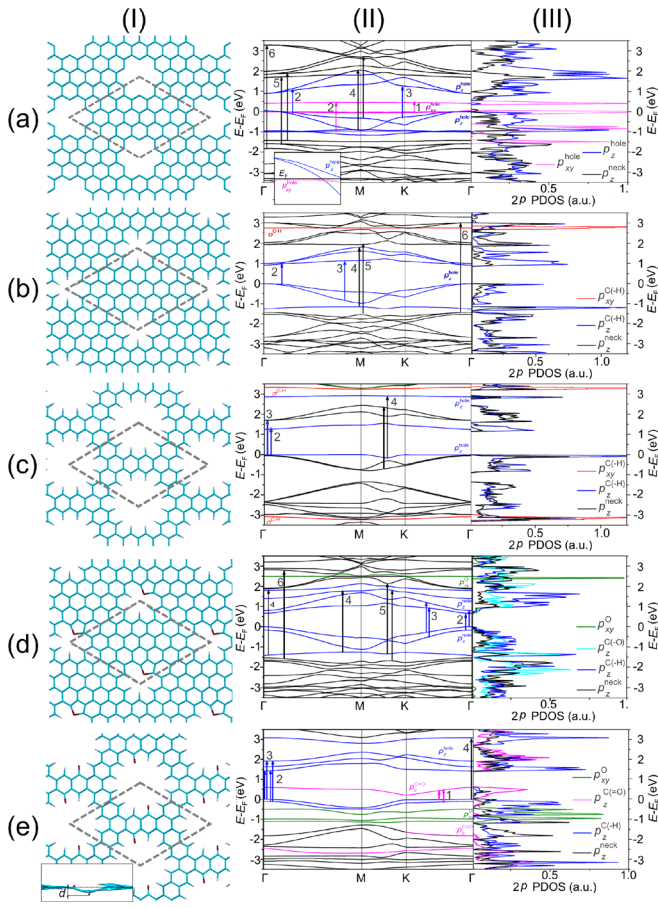
FIG. 2. Optimized structures (I), electronic band structures (II), and PDOS (III) of HG models: (a) 6-HG, (b) 6H-HG, (c) 24H-HG, (d) 6O^{ether}-HG, and (e) 24O^{ketonic}-HG. In panel I: cyan, gray, and red colors correspond to carbon, hydrogen, and oxygen; dashed rhombi show the unit cells. Inset in e-I: side view of 24O^{ketonic}-HG model; d is the out-of-plane deviation of the oxygen position from the initial one. Inset in a-II: band structure of the 6-HG model near the Fermi level around the Γ point. Arrows in panel II correspond to interband transitions responsible for absorption peaks labelled in Fig. 3.

$(p_z^{C=O}$ at the Fermi level of 24O^{ketonic}-HG model), and deep σ-states of passivated hole edges (σ^{C-H} in 6H-HG and 24H-HG models and p_{xy}^{O} in the 6O^{ether}-HG model). The bands of the second group are a little bit further away from the Fermi level (highlighted in blue in Fig. 2-II). These bands are associated with the atoms at the edges of the holes. Electronic density of the bands of the third group is evenly distributed on the atoms of HG models. These bands could be associated with graphene necks separating the holes.

Figure 3 compares the calculated optical spectra of the HG models with that of perfect graphene and experimental spectrum of the HG material. The absorption coefficient was calculated within random phase approximation starting from self-consistent field eigenvectors and eigenvalues for models using the post-processing epsilon.x code.[36] The graphene spectrum exhibits a single absorption peak at 4.0 eV, which arises from $\pi \rightarrow \pi^*$ transitions around the M point in the first Brillouin zone.[27,29,30,37,38] Neglecting many-body interactions is a
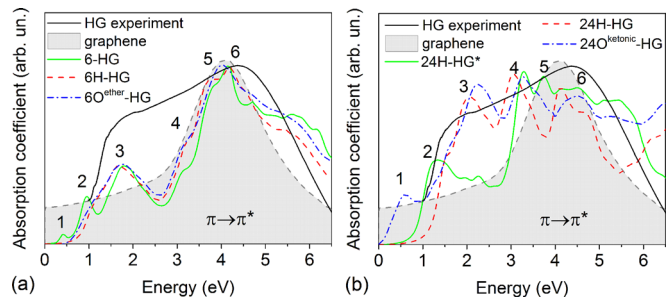
FIG. 3. Absorption coefficients of 6-HG, 6H-HG, and 6O^{ether}-HG (a) and 24H-HG, 24H-HG*, and 24O^{ketonic}-HG (b) in comparison with graphene and the HG sample. The numbers above the peaks refer to interband transitions labelled in Fig. 2-II.

reason for a redshift of the calculated absorption peak by 0.7 eV relative to experimental spectra of graphene[38] and TEG [Fig. 1(b)]. However, to catch the absorption peaks related to the electronic transitions between the conduction and valence band edges, we will discuss the origin of the absorption coefficient of the HG models starting from 0 eV.

The introduction of holes into the graphene layer results in broadening and splitting of the π-peak and appearance of new absorption bands, whose positions match the near-infrared (NIR) shoulder observed in the experimental spectrum of HG. To understand their origin, we determined the electronic transitions, which are principal for separate absorption bands of HG models. The transitions found are shown by arrows in Fig. 2(II), and the numbers near the arrows refer to numbers labelling the absorption peaks in Fig. 3. The example of such analysis is shown in Fig. 4(a). The sum of all single transition components matches the total absorption peaks very well. Further, the calculated PDOS results were used to correlate the electronic states, i.e., the absorption peaks, with local patterns of HG models (see supplementary material for details).

We start by considering the 6-HG model. In the low-energy range, the spectrum exhibits the peaks denoted as 1, 2, and 3. The first weak feature arises from transitions between pairs of p_{xy} states [purple arrow 1 in Fig. 2(a-II)], which are localized on edge carbon atoms with unpaired electrons [Fig. 4(b)]. Two absorption peaks denoted as 2 and 3 come from the transitions between the p_z states, localized in real-space on the carbyne-like hole edge [Fig. 4(c)]. When the energy is close to the excitation energy of graphene's plasmon, we note splitting of the single π-peak into several features, some of which are denoted as 4, 5, and 6. Analysis of the single-transition spectra and real-space localization of the initial and final states showed that these peaks are related to the optical transitions between the states mainly delocalized between the holes [Fig. 4(d)]. In general, graphene regions between holes resemble nanoribbons. Therefore, the splitting of neck-related band could be related to quantization of electronic states across the ribbon width.[39]

Hydrogenation of hole edge (transformation of model 6-HG to model 6H-HG) modifies the absorption spectrum slightly [Fig. 3(a)]. The most notable effect is the vanishing of peak 1, formed by unpaired electrons. The spectra of 6H-HG and 24H-HG* models [Figs. 3(a) and 3(b)], where graphene necks have the same width but the holes are different in size, are also alike except a minor difference in the shape. However, when the distance between the neighboring holes is reduced
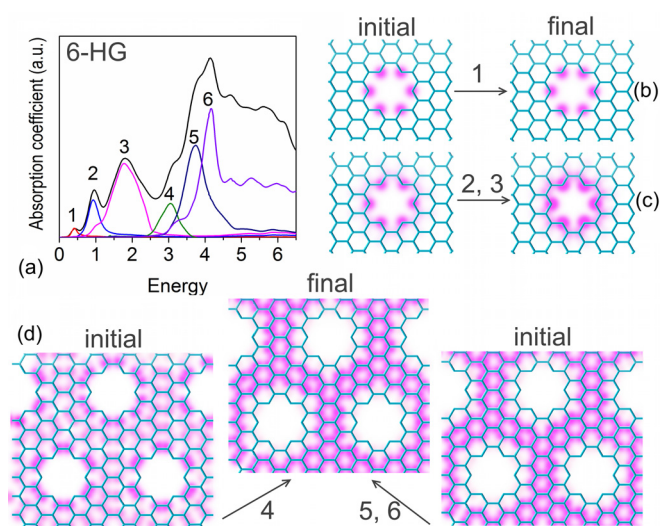
FIG. 4. Decomposition of the absorption spectrum of the 6-HG model into single transition contributions (a). Schematics of electron density maps for the initial and final states causing the single transition absorbance bands denoted as 1 (b), 2 and 3 (c), and 4, 5, and 6 (d).

down to one hexagon (24H-HG model), the absorbance changes drastically. In this case, the model is composed of just the hole edges without unperturbed graphene-like areas. Peak 2, which has the lowest energy in the spectrum of the 24H-HG model, comes from the transitions between states localized on a single hole. The transitions between the delocalized states of coupled holes [black lines in Fig. 2(c-II)] form intense peak 3. Substitution of hydrogen atoms attached to the hole edge by oxygen atoms affects the absorption spectrum of hydrogen-passivated HG models weakly except the appearance of the lowest-energy peak 1 ascribed to the p_z state of the C=O group for the 24O^{ketonic}-HG model [Fig. 3(b)].

The above analysis suggests that the additional NIR absorbance of HG arises from electronic states at the edges of nanoscale holes present in the graphene lattice. Variation of hole sizes and functionalization affects the spectrum slightly, while the occurrence of the holes separated by narrow necks could significantly broaden and enhance the edge-related absorption bands. The existence of the $\pi \rightarrow \pi^*$ absorption peak at *ca.* 4.7 eV in the experimental spectrum of the HG material indicates preservation of extended graphene areas between holes. That agrees with the TEM image and FFT pattern of the HG material [Fig. 1(a)]. The additional weak NIR shoulder in the absorption spectra of TEG and HRGO materials could be due to the presence of grain boundaries of TEG and HRGO domains and oxygenated holes in HRGO as well as basal oxygen groups according to Ref. 25.

In summary, a comparison of the experimental optical spectrum of HG containing *ca.* 1.6 at. % of residual oxygen with the spectra of HRGO and TEG reveals that the introduction of holes into graphene layers blueshifts the position of the absorption peak related to the $\pi \rightarrow \pi^*$ transition in graphene and produces a broad absorption between 1.2 and 2.2 eV. The changes in the optical spectra were reproduced by *ab initio* calculations and interpreted from joint analysis of dominant contributions of atomic orbitals of the HG models to the electronic states near the Fermi level and their involvement in the

optical interband transitions. Downshift of the honeycomb lattice-related optical peak could be due to quantum confinement effects and corrugation of graphene areas between the holes. The new low-energy band in the spectrum of HG is primarily determined by electron transitions between the states corresponding to carbon atoms from edges of the holes. Our results show that the optical spectrum of HG is strongly dependent on the distance between the holes and almost independent of both the hole size and the functionalization family. The presence of carbon atoms with dangling bonds or bound with oxygen by a double bond produces an absorption band at *ca.* 0.4 eV. Therefore, we suggest that the creation of nanoscale holes in graphene layers and control of their distribution could serve for tuning the NIR optical properties of graphene-based materials.

See supplementary material for details of the absorption coefficient calculation (general formula and single-transition analysis) and geometry of the 24H-HG* model.

REFERENCES

[1]Y. Lin, Y. Liao, Z. Chen, and J. W. Connell, Mater. Res. Lett. **5**, 209–234 (2017).
[2]C. Gómez-Navarro, J. C. Meyer, R. S. Sundaram, A. Chuvilin, S. Kurasch, M. Burghard, K. Kern, and U. Kaiser, Nano Lett. **10**, 1144–1148 (2010).
[3]Y. Hong, Z. Wang, and X. Jin, Sci. Rep. **3**, 3439 (2013).
[4]X. Wang, L. Jiao, K. Sheng, C. Li, L. Dai, and G. Shi, Sci. Rep. **3**, 1996 (2013).
[5]N. F. Yudanov, A. V. Okotrub, L. G. Bulusheva, I. P. Asanov, Y. V. Shubin, L. I. Yudanova, N. I. Alferova, V. V. Sokolov, N. N. Gavrilov, and A. V. Tur, J. Struct. Chem. **52**, 903–909 (2011).
[6]A. V. Okotrub, N. F. Yudanov, V. A. Tur, I. P. Asanov, Y. V. Shubin, D. V. Vyalikh, and L. G. Bulusheva, Phys. Status Solidi B **249**, 2620–2624 (2012).
[7]S. G. Stolyarova, E. S. Kobeleva, I. P. Asanov, A. V. Okotrub, and L. G. Bulusheva, J. Struct. Chem. **58**, 1180–1186 (2017).
[8]D. Kim, S. K. Yang, Y. S. Kim, H. Jung, and C. R. Park, Carbon **50**, 3229–3232 (2012).
[9]L. G. Bulusheva, S. G. Stolyarova, A. L. Chuvilin, Y. V. Shubin, I. P. Asanov, A. M. Sorokin, M. S. Mel'gunov, S. Zhang, Y. Dong, X. H. Chen, H. H. Song, and A. V. Okotrub, Nanotechnology **29**, 134001 (2018).
[10]T. G. Pedersen, C. Flindt, J. Pedersen, N. A. Mortensen, A.-P. Jauho, and K. Pedersen, Phys. Rev. Lett. **100**, 136804 (2008).
[11]A. Zhang, H. F. Teoh, Z. Dai, Y. P. Feng, and C. Zhang, Appl. Phys. Lett. **98**, 023105 (2011).
[12]V. H. Nguyen, M. C. Nguyen, H.-V. Nguyen, and P. Dollfus, J. Appl. Phys. **113**, 013702 (2013).
[13]J. Lee, A. K. Roy, J. L. Wohlwend, V. Varshney, J. B. Ferguson, W. C. Mitchel, and B. L. Farmer, Appl. Phys. Lett. **102**, 203107 (2013).
[14]G. Tang, Z. Zhang, X. Deng, Z. Fan, Y. Zeng, and J. Zhou, Carbon **76**, 348–356 (2014).
[15]H. Chen, K.-H. Jin, H. Guo, B. Wang, A. O. Govorov, X. Niu, and Z. Wang, Carbon **126**, 480–488 (2018).
[16]A. Sinitskii and J. M. Tour, J. Am. Chem. Soc. **132**, 14730–14732 (2010).
[17]X. Liang, Y.-S. Jung, S. Wu, A. Ismach, D. L. Olynick, S. Cabrini, and J. Bokor, Nano Lett. **10**, 2454–2460 (2010).
[18]J. Bai, X. Zhong, S. Jiang, Y. Huang, and X. Duan, Nat. Nanotechnol. **5**, 190–194 (2010).
[19]M. Kim, N. S. Safron, E. Han, M. S. Arnold, and P. Gopalan, Nano Lett. **10**, 1125–1131 (2010).
[20]M. Wang, L. Fu, L. Gan, C. Zhang, M. Rümmeli, A. Bachmatiuk, K. Huang, Y. Fang, and Z. Liu, Sci. Rep. **13**, 1238 (2013).
[21]A. Kazemi, X. He, S. Alaie, J. Ghasemi, N. M. Dawson, F. Cavsllo, T. G. Habteyes, S. R. J. Brueck, and S. Krishna, Sci. Rep. **5**, 11463 (2015).

[22]G. Eda, Y.-Y. Lin, C. Mattevi, H. Yamaguchi, H.-A. Chen, I.-S. Chen, C.-W. Chen, and M. Chhowalla, Adv. Mater. **22**, 505 (2010).

[23]C. Y. Kong, W.-L. Song, M. J. Meziani, K. N. Tackett II, L. Cao, A. J. Farr, A. Anderson, and Y.-P. Sun, J. Supercrit. Fluids **61**, 206–211 (2012).

[24]S. Zhang, Y. Li, Y. Kang, Y. Dong, S. Hong, X. Chen, J. Zhou, Y. V. Fedoseeva, I. P. Asanov, L. G. Bulusheva, and A. V. Okotrub, Carbon **108**, 461–470 (2016).

[25]M. Lundie, Ž. Šljivančanin, and S. Tomić, J. Mater. Chem. C **3**, 7632–7641 (2015).

[26]S. G. Stolyarova, M. A. Kanygin, V. O. Koroteev, Y. V. Shubin, D. A. Smirnov, A. V. Okotrub, and L. G. Bulusheva, Phys. Status Solidi B **255**, 1700262 (2018).

[27]O. V. Sedelnikova, L. G. Bulusheva, I. P. Asanov, and A. V. Okotrub, Appl. Phys. Lett. **104**, 161905 (2014).

[28]S. F. McKay, J. Appl. Phys. **35**, 1992 (1964).

[29]O. V. Sedelnikova, L. G. Bulusheva, and A. V. Okotrub, J. Chem. Phys. **134**, 244707 (2011).

[30]O. V. Sedelnikova, L. G. Bulusheva, and A. V. Okotrub, Fullerenes, Nanotubes, Carbon Nanostruct. **20**, 558 (2012).

[31]P. Giannozzi, S. Baroni, N. Bonini, M. Calandra, R. Car, C. Cavazzoni, D. Ceresoli, G. L. Chiarotti, M. Cococcioni, I. Dabo, A. D. Corso, S. de Gironcoli, S. Fabris, G. Fratesi, R. Gebauer, U. Gerstmann, C. Gougoussis, A. Kokalj, M. Lazzeri, L. Martin-Samos, N. Marzari, F. Mauri, R. Mazzarello, S. Paolini, A. Pasquarello, L. Paulatto, C. Sbraccia, S. Scandolo, G. Sclauzero, A. P. Seitsonen, A. Smogunov, P. Umari, and R. M. Wentzcovitch, J. Phys.: Condens. Matter **21**, 395502 (2009).

[32]J. P. Perdew and A. Zunger, Phys. Rev. B **23**, 5048 (1981).

[33]J. Nocedal and J. Wright, *Numerical Optimization* (Springer, New York, 1999).

[34]O. V. Sedelnikova, L. G. Bulusheva, and A. V. Okotrub, Synth. Met. **160**, 1848–1855 (2010).

[35]O. V. Sedelnikova, L. G. Bulusheva, and A. V. Okotrub, Phys. Status Solidi RRL **11**, 1600367 (2017).

[36]R. Colle, P. Parruccini, A. Benassi, and C. Cavazzoni, J. Phys. Chem. B **111**, 2800 (2007).

[37]O. V. Sedelnikova, C. P. Ewels, L. G. Bulusheva, and A. V. Okotrub, J. Struct. Chem. **59**, 870–876 (2018).

[38]L. G. Bulusheva, O. V. Sedelnikova, and A. V. Okotrub, Int. J. Quantum Chem. **116**, 270–281 (2016).

[39]D. H. Choe, J. Bang, and K. J. Chang, New J. Phys. **12**, 125005 (2010).